MODELING PULL-OUT BEHAVIOR OF THE DEFORMED REBAR EMBEDDED INSIDE THE REINFORCED CONCRETE

Kohar Yudoprasetyo[a], Bambang Piscesa[a*], Harun Alrasyid[a]

***Abstract**: This study presents the modeling of the pull-out behavior of deformed bars embedded inside the reinforced concrete element. The simulation uses an in-house finite element package called 3D-NLFEA. Sufficiently small solid elements that consider the frictional resistance and mechanical interlocking between the bar thread and the concrete matrix were used in the simulation. The effect of concrete compressive strength, cover thickness, and stirrup configuration on the pull-out capacity of the modeled specimens are investigated thoroughly. The modeling found out that the 3D-NLFEA package can capture the bond-fracture process at the interface between the bars and concrete. The fracture that occurs in the concrete was dominated by tensile splitting failure. The presence of stirrups that confined the concrete and restrained the crack propagation significantly influences the pull-out capacity, cracking pattern, and failure behavior at the bar interface with the concrete. The analysis results from 3D-NLFEA are also compared with the 3D-RBSM analysis results available in the literature. From the comparisons, it was found out that the 3D-NLFEA prediction was lower than the 3D-RSBM. From 3D-RSBM, the bond-slip response did not show residual load behavior, while from 3D-NLFEA, the residual load behavior was captured. As for the failure crack pattern, the prediction from 3D-NLFEA was somewhat similar to 3D-RSBM.*

Keywords: *Pull-out test, bond stress, tensile splitting fracture, frictional resistance*

INTRODUCTION

The concrete bond strength is a fundamental material property that controls the performance of the reinforced concrete structural element. This bond strength prevents the slip between the concrete and reinforcing bar such that it can works as a composite material. The bond stress developed at the interface is made up of three components: chemical adhesion, friction, and mechanical interaction [1]. The chemical adhesion was minimal and disappeared once the slip between the bar and concrete began.

In general, there are two types of bars typically used to reinforce the concrete material. There are plain and deformed bars. For the plain bars, the bond strength is mainly from friction and chemical adhesion. While for the deformed bars, the bond strength primarily depends on the mechanical interaction between the bar ribs (threads) and the concrete [1, 2]. In the case of deformed bars, the radial stresses generated due to the action of the bar thread can cause tensile stresses and develop micro and macro cracks in concrete [3].

One way to investigate the bar-concrete bond is to examine the bond stress-slip evolution via the classical pull-out test [4]. The pull-out capacity of the embedded bar inside the concrete is affected by many parameters such as the concrete compressive strength, the concrete cover thickness, and different stirrups configurations. The presence of stirrups was known to increase concrete's bond strength and ductility during the pull-out test. Once the concrete cracks, these stirrups restrained the crack growth and created confinement to the concrete core, increasing the pull-out resistance.

Lin et al. [5] did some experimental works to study the local bond stress-slip relationships of the embedded bar inside the RC elements. Some parameters being investigated are the effect of concrete compressive strength, the concrete cover thickness, and the stirrup configuration, which passively provide confinement to the concrete. Jin et al. [6] carried out a three-dimensional mesoscale model that focused on rebar bond-stress behavior, which considers the variation in concrete compressive strength, concrete cover thickness, and the stirrup configuration. Avadh et al. [7] evaluated the Lin et al. [6] test result using a three-dimensional rigid body spring model (3D-RBSM). From the brief review above, it can be concluded that the bond stress-slip behavior is complex and requires detailed analysis to predict the response.

This paper carried out numerical simulation using the 3D-NLFEA finite element package [8-10]. In the 3D-NLFEA simulation. The specimen is modeled with a tiny element to capture the crack propagation and model the bond-slip behavior between the concrete and the bar as accurately as possible. For verification purposes, the specimen geometry tested by Lin et al. [11] and modeled by Avadh et al. [7] are used and compared with the simulation result using 3D-NLFEA. The investigated parameters are the concrete compressive strength, concrete cover thickness, and the stirrup configurations similar to that of experimentally tested [7, 11].

RESEARCH SIGNIFICANCE

This paper presents numerical modeling on the pull-out behavior of the deformed bar embedded inside the concrete. The interaction between the bar and the concrete is modeled with a zero-thickness element and follows Mohr-Coulomb frictional model. The critical finding from this paper is that the bond-strength capacity of the embedded bar is affected by the concrete cover thickness, stirrup configurations, and the concrete compressive strength.

METHODOLOGY

A. GEOMETRY DETAIL AND 3D MODEL PREPROCESSING

Figure 1 shows the specimen geometry and the boundary condition tested by Avadh et al. [7]. The beam width and height are 150 mm and 250 mm, respectively. The beam length is 330 mm and is restrained in one direction at the

[a]Civil Engineering Department, Institut Teknologi Sepuluh Nopember, ITS Campus, Sukolilo, Surabaya 60111, Indonesia. Corresponding author email address: piscesa@ce.its.ac.id

left face. The debonding length near the restrained surface is 50 mm and on the other face is 80 mm. With the total debonding length of 130 mm, the effective bonded length is 200 mm. The longitudinal and stirrups bar diameters are 20 mm and 8 mm, respectively. The spacing of the stirrups is measured from the center-to-center of the bar. There are two spacing considered for the RC beam, which is 50 mm and 200 mm. For the stirrups with 50 mm spacing, there are three additional stirrups between the outer stirrups. The concrete cover thickness considered is 30 mm and 60 mm.

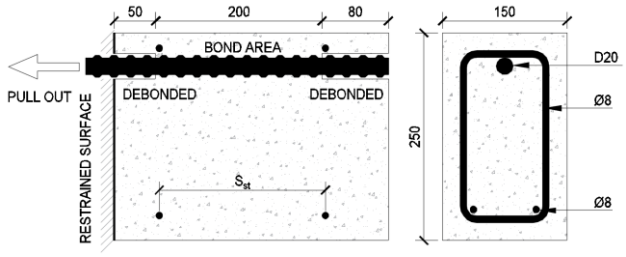

Figure 1 Specimen model geometry

Table 1 shows the configuration for the concrete cover thickness, stirrups pitch spacing, and the number of stirrups for each beam tested in [7]. There are six specimens modeled in this study.

Table 1 Model geometry parameters [7]

Specimen ID	Concrete cover (mm)	Stirrups spacing (mm)	No. of stirrups
LA0	30	0	0
LA1	30	200	2
LA4	30	50	4
LC0	60	0	0
LC1	60	200	2
LC4	60	50	4

Figure 2 shows the geometry modeling in the preprocessor phase using SALOME 9.3.0 [12]. As shown in Figure 2, all the concrete and rebar materials are modeled using the solid four nodes tetrahedral element with BBar element technology. The concrete and steel material interface is modeled using zero thickness cohesive element integrated using isoparametric formulation [13, 14]. The element size for the outer concrete layer is set to 10 mm, while at the concrete-rebar interface, the mesh size was reduced to 2 mm.

The boundary condition at the top face was fixed in all directions to represent the experimental pull-out test condition (see Figure 2c). At the top face of the longitudinal bar, a linearly increasing displacement along the Z-axis is applied to pull out the bar. The other concrete surfaces are free. All the meshed geometry, boundary condition, and material assignment are prepared in one input file in order to be able to be read using the 3D-NLFEA package [8, 9].

Avadh et al. [7] modeled the solid element using 3D polyhedral rigid elements connected to adjacent elements with one normal and two shear springs. The combination of these 3D polyhedral rigid elements and the springs become the 3D mesoscale rigid body spring model (3D-RBSM). Both the concrete and the steel material are modeled using 3D-RBSM. The use of three springs for each face was similar to that of the zero-thickness cohesive element used in 3D-NLFEA. One of the significant differences between the 3D-RBSM and 3D-NLFEA is the fracturing behavior in the concrete matrix, where the concrete matrix in 3D-NLFEA can undergo concrete crushing and tensile fracturing within the element. In 3D-RBSM, the fracturing in the concrete matrix will occur at the interface between the concrete matrices. In 3D-NLFEA, the similar spring model as in the zero-thickness cohesive element is only applied at the interface between the concrete and the steel reinforcing bar.

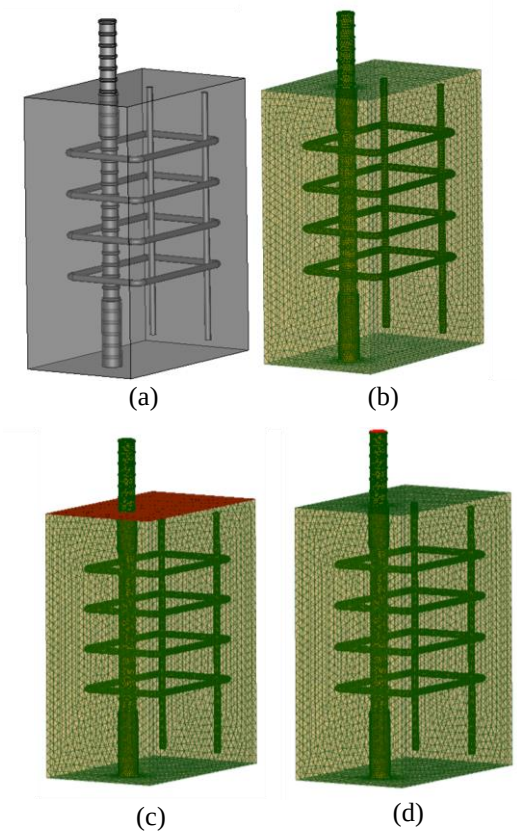

Figure 2. (a) 3D geometry model, (b) 3D meshed model, (c) Restrained BC at the concrete face (red-colored), (d) Displacement BC at the tip of the bar (red-colored)

Table 2 Total number of nodes, solid, and element

Specimen ID	Num. Of. Nodes	Num. Of. Solids	Num. Of. Elements
LA0	63,513	338,061	395,928
LA1	96,163	528,523	606,000
LA4	123,657	689,078	784,895
LC0	74,852	428,123	486,121
LC1	90,576	495,089	570,201
LC4	92,078	508,410	585,415

Table 3 Input material properties [7].

Material	f_c' (MPa)	f_t (MPa)	E (MPa)	f_y (MPa)
Concrete	28.05	2.53	24892.2	-
Rebar	-	-	200000	450
Stirrups	-	-	200000	378

Table 2 shows the total number of nodes, solids, and elements (includes the zero-thickness element) to construct the 3D model for each specimen. Table 3 shows the input material properties used in the modeling. the concrete compressive strength is 28.05 MPa, the concrete tensile strength is 2.53 MPa, and the concrete elastic modulus is

24892.2 MPa. The yield strength for the main longitudinal rebar is 450 MPa, while the stirrups are 378 MPa. The elastic modulus for both rebars and stirrups is 200 GPa.

B. CONSTITUTIVE MODEL OF MATERIALS AND CONTACT BEHAVIOR

The bar element which was modeled using solid element, follows the J_2 material model (Von Mises criterion). An Elastic-perfectly plastic stress-strain model was adopted. A multi-surface plasticity model is used for the concrete material. In the multi-surface plasticity model, the three-parameter criterion for the failure surface proposed by [15] was modified [16] to improve its peak and residual strengths for high-strength concrete. The modification in [16] introduced a new frictional driver parameter that adjusted the peak stress prediction based on Attard and Setunge model and residual stress for concrete under confined based on model.

A zero-thickness cohesive element that obeys the Mohr-Coulomb law is used to model the interaction between the concrete and steel rebar materials. The separation between the materials occurs when the normal stress is greater than the tensile strength of the bond. The equation for the Mohr-Coulomb failure surface can be written as follows:

$$f = \tau_1^n + \tau_2^n - \left(c - \sigma_n \tan\phi\right)^n + \left(c - \xi \tan\phi\right)^n \quad (1)$$

In Eqn.(1), the shear stresses are represented by two shear strengths (τ_1 and τ_2) that are perpendicular to each other on the surface plane. The cohesive strength (c) is determined as the shear stress when the slip occurs at zero normal stress (σ_n). The shear strength of the interface is governed by the normal strength acting on the normal vector to the plane of the interface. The shear strength is also affected by the surface roughness between the contact surface. The surface roughness is controlled by setting the internal friction angle (ϕ) in Eqn.(1).

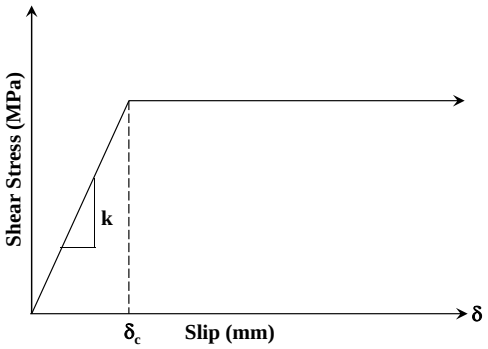

Figure 3 Shear-slip model for the zero-thickness cohesive element at the interface

Figure 3 shows the shear-slip model for the zero-thickness cohesive element at the interface. As shown in Figure 3, τ_c is the vector of shear stress at the onset of slip and is measured as the cohesive shear stress (c) in the Mohr-Coulomb formulation when the normal stress is zero. The parameter δ_c is the elastic deformation up to the point where the slip will occur. Once the slip occurs, the shear stress is assumed to be constant. When fracturing in the concrete material occurs, the surrounding element at the interface cannot maintain the threshold slip shear stress and eventually lead to elastically unloading behavior at the interface. Penetration between materials can be avoided by setting the value for the normal modulus of the zero-thickness element equal to the concrete modulus. The tangential modulus of the zero-thickness element is set one-tenth of its normal modulus.

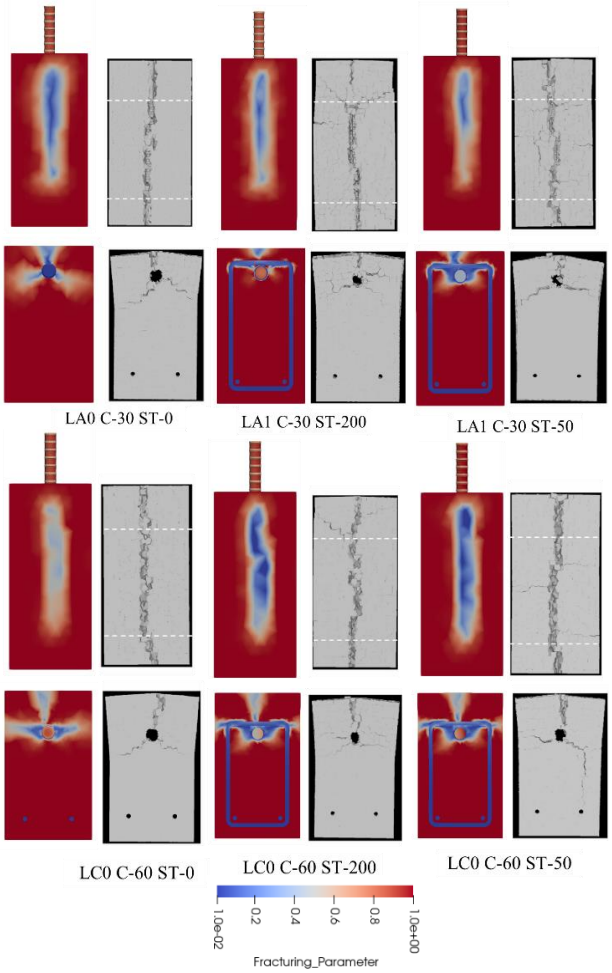

Figure 4 Concrete fracturing pattern after the peak stress reached

ANALYSIS RESULTS AND DISCUSSIONS

A. CONCRETE FRACTURING PATTERN AND ITS PROCESS

Figure 4 showed the concrete fracturing pattern when the peak bond stress was reached for both packages (3D-NLFEA and 3D-RSBM). The cracks on the outer surface of the concrete were clearly seen for all the specimens. The concrete fracturing is dominated by tensile splitting failure. When the stirrups are not present to restrain the crack growth, two main cracks grow diagonally away from the pull-out bar. While when the stirrup presents, the crack follows the stirrup direction, clearly indicating the stirrups' activation to prevent the crack growth. The crack in the diagonal direction is still visible (not pronounced), and the concrete fractures in the perimeter of the pull-out bar are spreading, which identifies a combination of tensile splitting failure and local concrete crushing. It is worth mentioning that the failure pattern generated by 3D-NLFEA is almost the same as the model used using 3D-RBSM.

In Figure 5, the mechanical interaction that works on the interface and possible failure patterns are shown. Assuming tensile force in the bar goes in the left direction, the concrete at the front of the rib would have compression stresses and the possibility of concrete crushing. On the other hand, the concrete at the back of the rib would delaminate. The non-compatible deformation between the concrete that crush (compacted) and delaminate due to pulling and slippage modes (with the bar separated) creates a diagonal crack from the edge of the front rib.

This diagonal crack, viewed as a cylindrical coordinate with the center of the bar as the origin, would have a conical wedge-shaped pile of crushed concrete. As the damage grows, one can have the global slip surface, which combines the concrete crushing failure and the delamination of the concrete. Once the conical wedge-shaped concrete no longer has the strength to transfer the stress from the bar to the surrounding concrete, the bond strength of the concrete drops significantly. This slip surface by friction can be used to compute the pull-out capacity of the deformed bar, as shown in Figure 5.

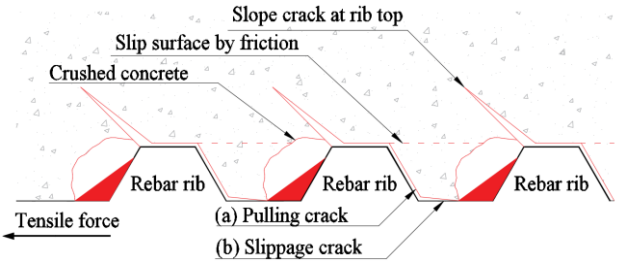

Figure 5 Mechanical interaction at the interface and possible failure patterns

B. BOND STRESS-SLIP RELATIONSHIP

Figure 6 shows the bond-stress prediction using 3D-NLFEA as a function of the bar tip displacement displaced during simulation. The bond stress can be computed using the tensile force at the displacement tip must be divided by the slip surface area. Therefore, the bond stress can be computed as follows:

$$\tau = \frac{F}{\pi d l} \tag{2}$$

Where F is the tensile force at the bar's tip, d the nominal diameter of the steel bar, l is the bonded length.

In Figure 6, the behavior of the bond stress-displacement relationship from the 3D-NLFEA simulation has a smooth transition from the proportional limit until the peak load is reached. Once the peak load is reached, the response softens until the residual strength of the bond stress is gone. This residual strength is not flat but clearly shows a decaying sign with a low softening modulus over time. This low decaying bond strength can be associated with gradual concrete crushing when forming the slip surface by friction, as shown in Figure 5.

Figure 8 shows the comparisons of the load-displacement response from the 3D-NLFEA and 3D-RSBM (obtained from [7]). Among all the investigated specimens, only in specimen LA0 the 3D-NLFEA prediction of load carrying capacity was higher than the prediction from 3D-RSBM. The 3D-NLFEA prediction for the rest of the specimens was more conservative than the 3D-RSBM. The load-displacement response from 3D-NLFEA can show a complete response which consists of peak load, softening response, and residual load with low decaying softening modulus.

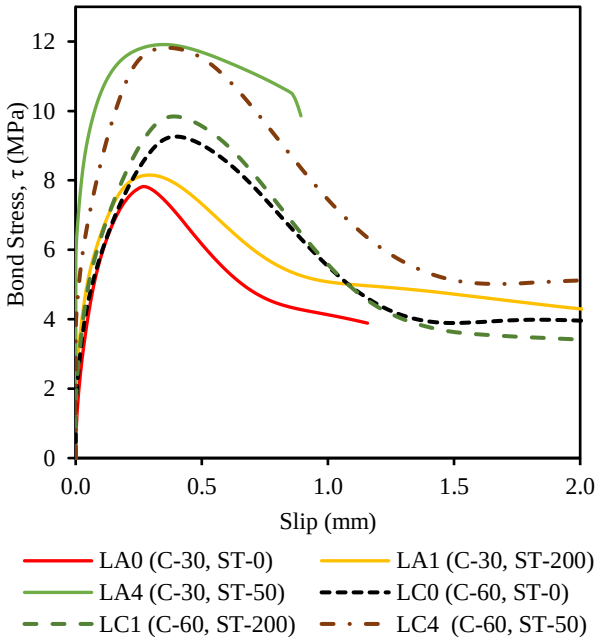

Figure 6 The bond stress-tip displacement relationship of the simulation results.

From the 3D-NLFEA simulation, specimen LA4 performed the best compared to the other specimen. The LA4 peak load prediction was significantly higher than LA1 and only slightly lower than LC4. The residual load capacity for LA4 was also quite significantly high. The residual load level for LC4 did not differ much from LC1 and LC0. However, the peak load for LC4 did show some improvement over LC1 and LC0 but was not significant. These findings indicate that low-strength concrete is more beneficial when confined compared to high-strength concrete. The proposition effect of confinement can be normalized with the concrete strength. Since the same stirrup configuration would give a similar confinement level, normalizing the confinement level with the concrete strength would give higher strength enhancement for low strength concrete.

C. EFFECT ON THE VARIATION OF THE CONCRETE COVER THICKNESS

In Figure 6, it is clearly seen that the concrete cover thickness significantly affects the peak bond strength. With the increase of concrete cover thickness from 30 to 60 mm (for the bar embedded inside the plain concrete block), the peak bond strength increases from 8 to 10 MPa (approximately 20% increase in bond strength capacity). The initial stiffness of the bond stress–tip displacement was not affected by the concrete cover thickness. However, the softening slopes after the peak bond strength were found to be higher for the specimen with a thicker concrete cover.

Figure 7 shows the plane and 3D volume views of the fracturing area for LA4 and LC4 specimens. As shown in Figure 7, the fractured volumes were more significant for the specimen with a thicker concrete cover. These more prominent areas of fractured volume explain the higher

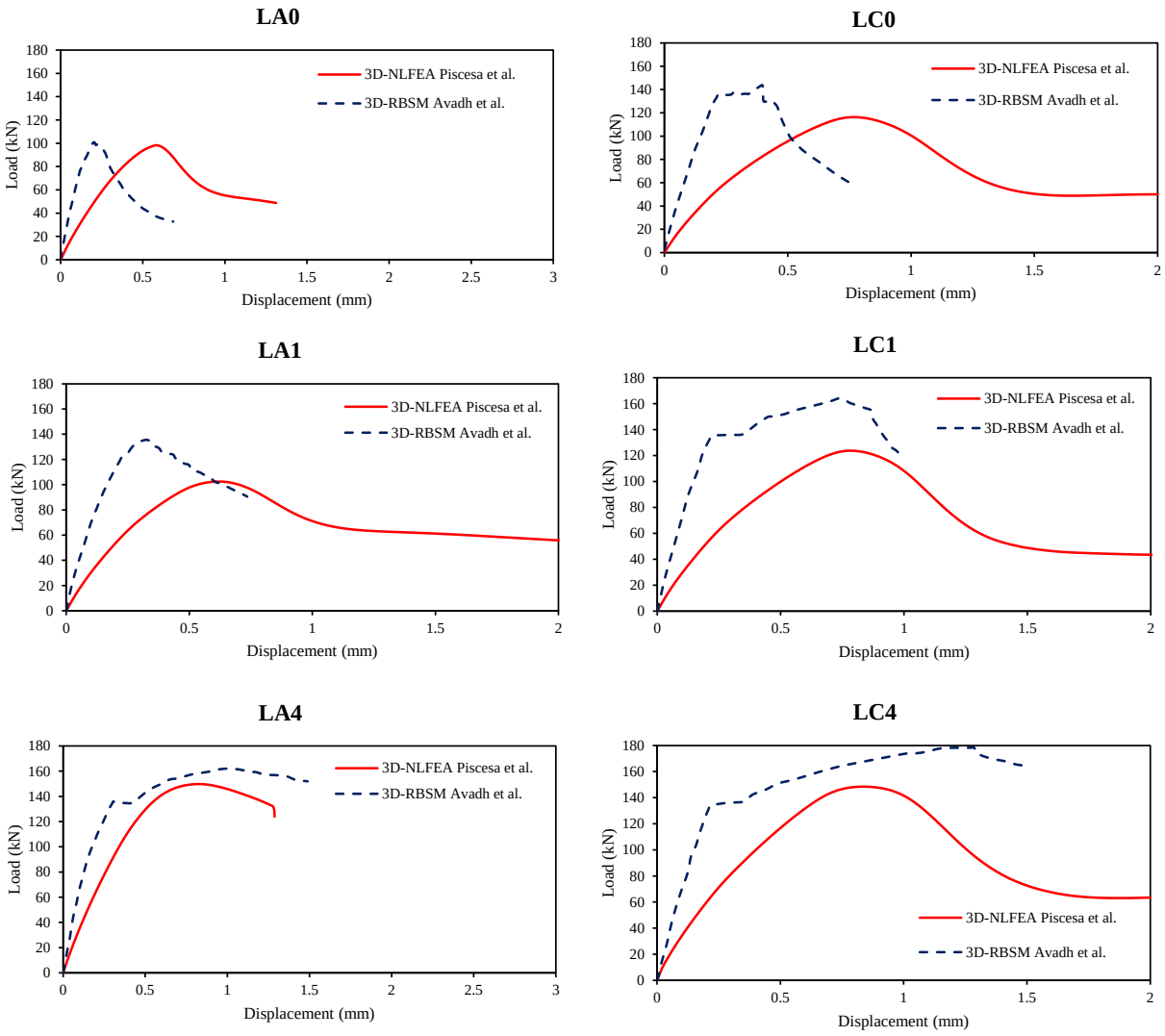

Figure 8 Load-displacement of the simulation results by 3D-NLFEA (with zero thickness cohesive element) and 3D-RBSM (with rigid body spring model)

peak bond strength of the specimen with 60 mm thick of the concrete cover.

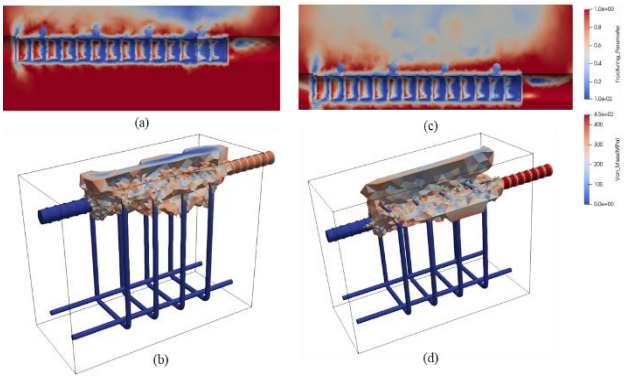

Figure 7 Concrete fractured volume (at displacement 0.6 mm) (a) Plane view for LA4, (b) 3D volume view for LA4, (c) Plane view for LC4, (d) 3D volume view for LC4.

D. EFFECT OF VARIATION IN CONCRETE STRENGTH

One plain specimen with a 60 mm thick concrete cover (LC4) is investigated to study the effect of variation in concrete strength. The concrete compressive strength considered is 20, 28, 45, and 70 MPa. Figure 9 shows the bond stress-slip relationship with varying concrete compressive strength. As shown in Figure 9, the concrete compressive strength affects the bond strength capacity and changes the hardening behavior of the bond stress-slip response. Lower concrete strength gives lower bond strength capacity and vice versa. Higher concrete strength shows more linear hardening behavior, while lower concrete strength shows more curved hardening behavior.

One interesting finding is that for 45 and 70 MPa concrete, the flat plateau of bond stress was captured from the analysis. The yielding of the reinforcement causes the flat plateau. This softening behavior may be caused by crushing. However, for 45 MPa concrete, the flat plateau softens when the slip reaches about 1.1 mm. and fracturing concrete when excessive bar deformation takes place. When the rebar yields, due to the nature of J_2 plasticity model, it would give an equivalent Poisson's ratio of 0.5. This condition means that the bar would shrink at a faster rate than when it is still in elastic condition. With more rapid volume shrinking in the bar, the delamination due to loss of the bond at the surface between the bar and concrete

would be more pronounce. With the progression delamination and crushing of concrete near the ribs, softening response in the bond stress-slip relationship was expected.

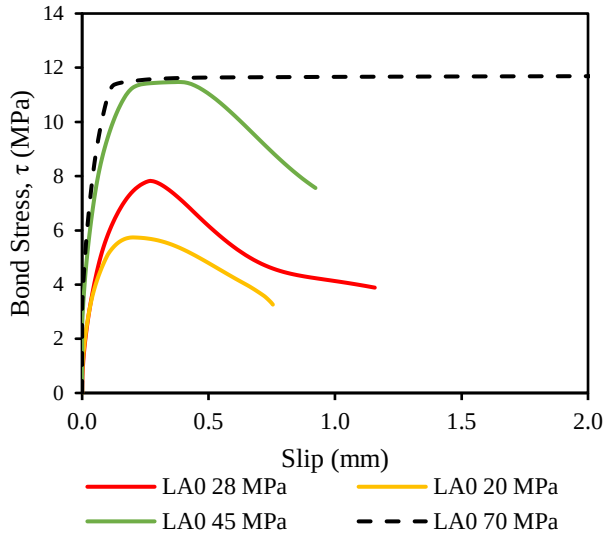

Figure 9 bond stress-slip relationship with varying concrete compressive strength

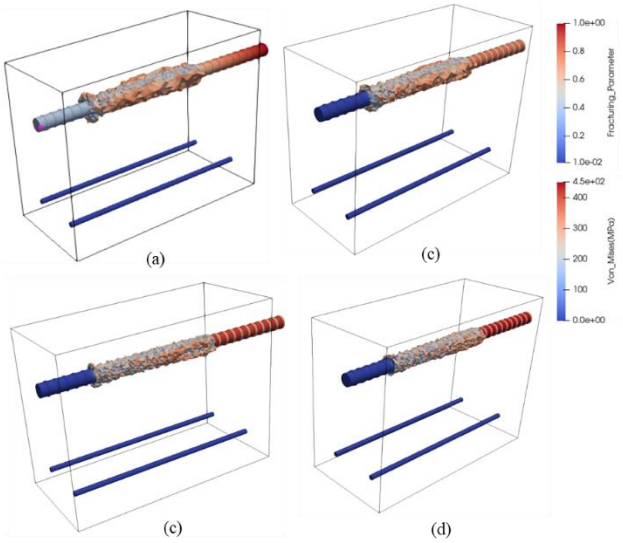

Figure 10 Concrete fractured volume (at displacement 0.6 mm), (a) 20 MPa concrete, (b) 28 MPa concrete, (c) 45 MPa concrete, (d) 70 MPa concrete

Figure 10 shows the fractured volume regions for 20, 38, 45, and 70 MPa concretes. The fractured volume regions were captured when the tip displacement was equal to 0.6 mm. The fractured volume for lower concrete strength was observed to have a larger fractured volume than the higher strength one. This can be well understood since the tensile strength for high-strength concrete is higher than the lower-strength concrete. Hence, the damage that occurred in the concrete is much less under similar tensile forces.

E. EFFECT OF VARIATION IN STIRRUPS

Figure 11 shows the bond stress-slip response for three specimens (LA0, LA1, and LA4) with varying stirrups configurations. As shown in Figure 11, the presence of stirrups increases the bond strength capacity of the concrete. Only one anomaly was found from the simulation where the softening modulus at the residual decaying bond stress response was found to be slightly higher for plain concrete compared to the specimen with 200 mm pitch spacing.

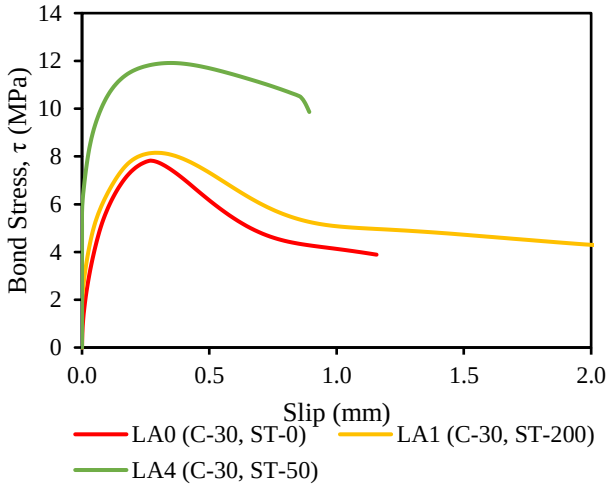

Figure 11 bond stress-slip relationship with varying stirrups configuration

CONCLUSIONS

Numerical modeling of the pull-out behavior of the embedded bar inside the concrete has been investigated. The study was carried out to investigate the affecting parameters to the pull-out capacity and the bond-stress relationship of the embedded bar. The affecting parameter being investigated are the concrete cover thickness, the stirrup configurations, and the concrete compressive strength. An in-house 3D-NLFEA package was used in the simulation. Zero thickness element with Mohr-Coulomb criterion was used to model the bond between the concrete and reinforcing bar. For comparison purposes, simulation results available in the literature using 3D-RSBM are included in the discussion to compare the failure cracking patterns and the load-deformation relationship for all the investigated specimens.

The comparisons of the bond-slip response from 3D-NLFEA and 3D-RSBM were compared. From the comparisons, it was found out that the 3D-NLFEA prediction was lower than the 3D-RSBM. From 3D-RSBM, the bond-slip response did not show residual load behavior, while from 3D-NLFEA, the residual load behavior was captured. As for the failure crack pattern, the prediction from 3D-NLFEA was somewhat similar to 3D-RSBM.

The analysis found that the pull-out capacity is greatly affected by the presence of stirrups that restrained the crack growth during the pull-out. The tighter the pitch spacing of the stirrups, the higher peak and residual load of the bond stress was obtained. One interesting finding with the variation of stirrups combined with different concrete strength was that the specimen with low strength concrete benefitted more from confinement rather than high strength concrete specimen. This can be identified by looking at higher residual bond stress obtained from the simulation.

The concrete strength was found to affect the bond stress-slip response where higher strength concrete adjusts

the hardening behavior of the bond stress-slip to be steeper than the lower strength ones. For 20 and 28 MPa concretes, the failure was governed by concrete fracturing and crushing. These concrete fracturing and crushing can be identified when the bond stress softens, and the stress in the bar is elastically unloading. For 45 MPa concrete, the rebar was found to be yielded. However, as the fracture and damage in concrete progressed, the concrete crushed and fractured, which eventually led to softening bond stress-slip response and the stress in the bar unloads. For 70 MPa concrete, a similar finding was obtained with 45 MPa concrete, but the yield plateau was found to be longer.

REFERENCES

[1] H. Lin, Y, Zhao, P. Feng, H. Ye, J. Ozbolt, C. Jiang, and J. Q. Yang, "State-of-the-art review on the bond properties of corroded reinforcing steel bar," *Construction and Building Materials*, vol. 213, pp. 216-233, 2019.

[2] P. Chana, "A test method to establish realistic bond stresses," *Magazine of Concrete Research*, vol. 42, no. 151, pp. 83-90, 1990.

[3] R. Tepfers, "Cracking of concrete cover along anchored deformed reinforcing bars," *Magazine of Concrete Research*, vol. 31, no. 106, pp. 3-12, 1979.

[4] A. M. Diab, H. E. Elyamany, M. A. Hussein, and H. M. Al Ashy, "Bond behavior and assessment of design ultimate bond stress of normal and high strength concrete," *Alexandria Engineering Journal*, vol. 53, no. 2, pp. 355-371, 2014.

[5] H. Lin, Y. Zhao, J. Ozbolt, P. Feng, C. Jiang, and R. Eligehausen, "Analytical model for the bond stress-slip relationship of deformed bars in normal strength concrete," *Construction and Building Materials*, vol. 198, pp. 570-586, 2019.

[6] L. Jin, M. Liu, R. Zhang, and X. Du, "3D meso-scale modelling of the interface behavior between ribbed steel bar and concrete," *Engineering Fracture Mechanics*, vol. 239, p. 107291, 2020.

[7] K. Avadh, P. Jiradilok, J. E. Bolander, and K. Nagai, "Mesoscale simulation of pull-out performance for corroded reinforcement with stirrup confinement in concrete by 3D RBSM," *Cement and Concrete Composites*, vol. 116, p. 103895, 2021.

[8] B. Piscesa, M. M. Attard, D. Prasetya, and A. K. Samani, "Modeling cover spalling behavior in high strength reinforced concrete columns using a plasticity-fracture model," *Engineering Structures*, vol. 196, p. 109336, 2019.

[9] B. Piscesa, M. M. Attard, and A. K. Samani, "3D Finite element modeling of circular reinforced concrete columns confined with FRP using a plasticity based formulation," *Composite Structures*, vol. 194, pp. 478-493, 2018.

[10] B. Piscesa, "Modeling confined concrete using plasticity formulation," PhD. Thesis, School of Civil and Environmental Engineering, The University of New South Wales, Sydney, Australia, 2018.

[11] H. Lin, Y. Zhao, J. Ožbolt, and H.-W. Reinhardt, "Bond strength evaluation of corroded steel bars via the surface crack width induced by reinforcement corrosion," *Engineering Structures*, vol. 152, pp. 506-522, 2017.

[12] SALOME, "The open-source platform for Numerical Simulation," *Salome Platform*, 01-Jan-2022. [Online]. Available: https://www.salome-platform.org/.

[13] R. E. Goodman, R. L. Taylor, and T. L. Brekke, "A model for the mechanics of jointed rock," *Journal of Soil Mechanics & Foundations Div*, vol. 94, no. SM3, pp. 637-659, 1968.

[14] G. Bfer, "An isoparametric joint/interface element for finite element analysis," *International journal for numerical methods in engineering*, vol. 21, no. 4, pp. 585-600, 1985.

[15] P. Menetrey and K. Willam, "Triaxial failure criterion for concrete and its generalization," *ACI structural Journal*, vol. 92, no. 3, pp. 311-318, 1995.

[16] B. Piscesa, M. Attard, A. Samani, and S. Tangaramvong, "Plasticity constitutive model for stress-strain relationship of confined concrete," *ACI Structural Journal*, vol. 114, no. 2, pp. 361-371, 2017.